Journal of
Computational and Theoretical Nanoscience
Vol. 4, 1–10, 2007

The Effect of Defects on the Mechanical Behavior of Silver Shape Memory Nanowires

Changjiang Ji and Harold S. Park*

Department of Civil and Environmental Engineering, Vanderbilt University, Nashville, TN 37235-1831, USA

We present atomistic simulations of the uniaxial tensile deformation of silver shape memory nanowires to investigate the effects of initial defects on the resulting thermomechanical behavior. In particular, the focus of the work is on investigating the unique atomistic deformation mechanisms that are observed during the tensile loading as a result of the initial defects, while correlating that behavior to the measured mechanical properties of the shape memory nanowires. In particular, wires with initial defects show a non-constant stress state during the ⟨110⟩/{111} to ⟨100⟩/{100} reorientation due to the presence of multiple propagating twin boundaries, as well as reductions in transformation stresses and strains due to the presence of the initial defects. Under most circumstances, the wires with initial defects still tend to exhibit complete reversibility between the ⟨110⟩/{111} and ⟨100⟩/{100} orientations, and thus the shape memory effect. Comparisons are made to defect-free shape memory nanowires to illustrate the relative mechanical performance of each structure.

Keywords: Shape Memory, Pseudoelasticity, Silver Nanowires, Atomistic Simulation, Initial Defects.

RESEARCH ARTICLE

1. INTRODUCTION

Of the multitude of experimentally synthesized and studied nanoscale structural materials, metallic and semiconducting nanowires appear to be one of the most promising for functionalization in future nanoscale machines and devices. Nanowires have been proposed for many important nanoscale applications, including biosensing,[1] as interconnects in future nanoscale electronics,[2] in photonics,[3] and many others.[4]

From a mechanics perspective, nanowires have many desirable properties, including yield stresses, yield strains and fracture strains that far exceed those found in the corresponding bulk material. These properties have been obtained through experimental[5–7] and theoretical investigations into the uniaxial tensile deformation of nanowires. Nanowires with a ⟨100⟩/{100} orientation have been studied most frequently;[8–19] other orientations, such as ⟨110⟩ or ⟨111⟩ have also been studied,[20–25] though the literature is not as extensive.

Recently, metal nanowires have been found to undergo phase transformations and structural reorientations that are surface stress driven, with additional dependencies on size, thermal energy, and material properties. For example, gold nanowires were found to phase transform from FCC to body-centered tetragonal (BCT) if the wire cross sectional length is below about 2 nm.[26,27] ⟨100⟩/{100} FCC metal nanowires were found to reorient to a lower energy ⟨110⟩ configuration with {111} side surfaces and a rhombic cross section by various researchers.[25,28–33] The reorientation is caused by intrinsic surface stresses[34] that cause instability of the ⟨100⟩/{100} orientation if the wire cross sectional length is sufficiently small, driving the reorientation to the lower energy ⟨110⟩/{111} orientation. The energetics of the reorientation have been confirmed both by experiment,[35] and by recent density functional and tight binding calculations,[36] which show that copper, nickel, and silver nanowires do in fact reorient from ⟨100⟩/{100} to ⟨110⟩/{111} under their own surface stresses if the wire diameter is less than about 2 nm.

Of significant interest, the reoriented ⟨110⟩/{111} nanowires were shown to exhibit both shape memory and pseudoelastic behavior[29–32,37] that has previously been seen only in bulk, polycrystalline shape memory alloys such as nickel titanium (NiTi).[38] The shape memory effect in nanowires is a purely nanoscale phenomenon, and is made possible due to the fact that intrinsic surface stresses, which are insignificant at the macroscale, are substantial at the nanoscale and continuously drive the reorientation from higher energy ⟨100⟩/{100} to lower energy ⟨110⟩/{111} configurations.

*Author to whom correspondence should be addressed.

Polycrystalline shape memory alloys (SMAs) are typically utilized as essentially one-dimensional structures; therefore, much of the experimental work characterizing their thermomechanical behavior has focused on uniaxial deformation.[38–40] For nanowires, previous work has been performed by the authors on the uniaxial thermomechanical deformation of silver shape memory nanowires.[32] However, one critical issue that has not been considered to-date is the influence of defects formed during the $\langle 100\rangle/\{100\}$ to $\langle 110\rangle/\{111\}$ reorientation on the subsequent thermomechanical properties and deformation behavior of the shape memory nanowires; previous investigations into the shape memory and pseudoelastic behavior were performed on idealized, defect-free nanowires.[29–32]

Therefore, the purpose of this paper is to characterize the influence of pre-existing defects on the thermomechanical behavior and properties of silver shape memory nanowires. Due to the likelihood of future difficulty in synthesizing defect-free nanowires, and due to the fact that individual lattice or surface imperfections can dramatically degrade the mechanical strength of nanoscale materials, such investigations are necessary to assess the practical potential of these novel shape memory materials. By performing atomistic simulations of the tensile deformation of $\langle 110\rangle/\{111\}$ nanowires with initial defects, we quantify the effects of the pre-existing defects on the observed atomistic deformation mechanisms, while relating these mechanisms to the nanowire strength and mechanical properties. Comparisons to defect-free nanowires and polycrystalline shape memory alloys are made for further insight.

2. SIMULATION METHODS

Classical molecular dynamics (MD)[41] simulations were performed modeling the atomic interactions using the embedded atom method (EAM)[42, 43] as the underlying atomic interaction model. For the EAM, the total energy U for a system of atoms can be written as

$$U = \sum_{i}^{N}\left(F_i(\bar{\rho}_i) + \frac{1}{2}\sum_{j\neq i}^{N}\phi_{ij}(R_{ij})\right) \quad (1)$$

where the summations in (1) extend over the total number of atoms N in the system, F_i is the embedding function, $\bar{\rho}_i$ is the electron density at atom i, ϕ_{ij} is a pair interaction function, and R_{ij} is the distance between atoms i and j. The specific potential utilized in this work for silver was that developed by Voter and Chen,[44] which was fit to cohesive energy, equilibrium lattice constant, bulk modulus, cubic elastic constants, and the unrelaxed vacancy formation energy, bond length and bond strength of the diatomic molecule.

Square cross section gold $\langle 100\rangle/\{100\}$ nanowires were created out of a bulk FCC crystal with {100} surface orientations. The wires were all 20.45 nm long in the z-direction, with cross sectional lengths of 2.045 nm in the x and y-directions. Because the shape memory effect is obtained in nanowires through reversibility between the $\langle 100\rangle/\{100\}$ and $\langle 110\rangle/\{111\}$ orientations, the $\langle 100\rangle/\{100\}$ to $\langle 110\rangle/\{111\}$ reorientation was achieved by fixing the ends of the wires to move only in the z-direction along with heating to 500 K using a Nosé-Hoover thermostat[45, 46] with a time step of 0.001 ps.

As was illustrated by multiple researchers,[28–32] there exists a critical reorientation temperature T_c which is directly proportional to the wire cross sectional length; T_c increases with the wire cross sectional length as the surface stresses decrease proportional to the wire cross sectional length. Previous studies[30, 31] have shown that the shape memory effects are achieved by stress-inducing a reorientation from $\langle 110\rangle/\{111\}$ to $\langle 100\rangle/\{100\}$ at a temperature less than T_c. By subsequently heating the stress-induced $\langle 100\rangle/\{100\}$ wire above T_c, reorientation back to $\langle 110\rangle/\{111\}$ occurs thus illustrating the shape memory effect. If the stress-induced reorientation occurs at a temperature greater than T_c, then the resulting $\langle 100\rangle/\{100\}$ wire will be unstable under its surface stresses, and pseudoelastic unloading back to the $\langle 110\rangle/\{111\}$ configuration will occur.

The focus of this work will therefore be on the uniaxial tensile deformation of the $\langle 110\rangle/\{111\}$ nanowires with initial defects. The $\langle 110\rangle/\{111\}$ wires that were tensile loaded were obtained by annealing the reoriented $\langle 110\rangle/\{111\}$ nanowires to three different temperatures using the Nosé-Hoover thermostat: 30 K, 200 K, and 400 K. These temperatures were chosen as representative values that are less than or equal to the critical reorientation temperature ($T_c = 400$ K) for the wire size chosen for this paper. The annealed wires were then loaded in tension in the z-direction at the three temperatures and strain rates of $\dot{\epsilon} = 1\times10^8$, 1×10^9, 1×10^{10} by fixing one end of the wire, creating a ramp velocity profile which went from zero at the fixed end to a maximum value at the free end, then pulling the free end at the maximum value. The ramp velocity profile was utilized to avoid the emission of shock waves from the loading end of the wire. All references to strain rate in this paper will be in units of s^{-1}. As with any MD simulation, the strain rates imposed during loading are higher than are generally observed experimentally. Thus, we have simulated the material response of the annealed $\langle 110\rangle/\{111\}$ nanowires across three decades of accessible MD loading rates to isolate the characteristic mechanical properties. The equations of motion were integrated in time using a velocity Verlet algorithm, and all simulations were performed using the Sandia-developed code Warp.[47, 48]

For each temperature and strain rate, the uniaxial tensile deformation of the annealed $\langle 110\rangle/\{111\}$ nanowires was performed both with and without Nosé-Hoover thermostatting; the thermostatting is utilized to model isothermal deformation by idealized heat transfer to a

surrounding medium, while simulations without thermostatting model adiabatic deformation. These idealized conditions were chosen as transient heat transfer effects have been shown to have a significant effect on the mechanical behavior of polycrystalline SMAs.[39, 49] For the remainder of the paper, we will refer to the thermostatted simulations as isothermal, while the non-thermostatted simulations will be referred to as adiabatic.

3. SIMULATION RESULTS AND DISCUSSION

3.1. ⟨100⟩/{100} to ⟨110⟩/{111} Reorientation

We first illustrate the ⟨100⟩/{100} to ⟨110⟩/{111} reorientation at 500 K. While this reorientation has been documented by various researchers,[25, 28–32] we illustrate here the process leading to the formation of the ⟨110⟩/{111} nanowires with interior defects. This reorientation process is driven by intrinsic surface stresses that allow the ⟨100⟩/{100} nanowire to reduce its surface energy by reorienting to a ⟨110⟩ orientation with low energy {111} side surfaces. The reorientation process from ⟨100⟩/{100} to ⟨110⟩/{111} is illustrated in Figures 1 and 2, which show the process leading to ⟨110⟩/{111} nanowires that do and do not contain interior defects. Both figures show side by side snapshots of the nanowire potential energy along with the atoms visualized using the centrosymmetry parameter,[50] which is a measure of local atomic coordination; a value of zero indicates a bulk, fully-coordinated atom while values increasingly greater than zero indicate the presence of lattice defects such as dislocations, stacking faults, and twins.

The reorientation process leading to the ⟨110⟩/{111} silver nanowire with parallel interior {111} stacking faults

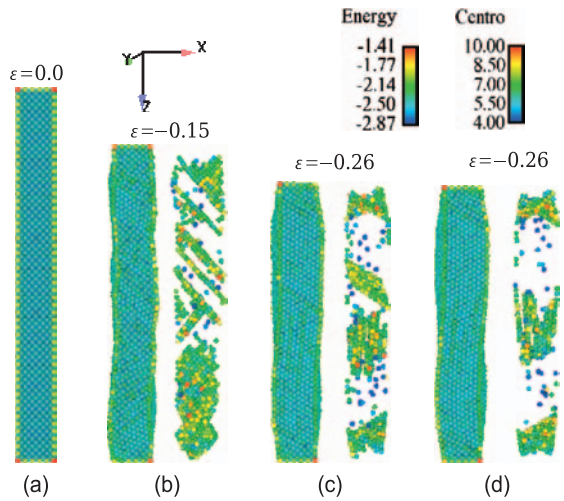

Fig. 1. The reorientation of an initially defect-free ⟨100⟩/{100} silver nanowire to a ⟨110⟩/{111} orientation containing interior parallel {111} stacking faults at 500 K. Units of potential energy are in eV, centrosymmetry is defined in Ref. [50].

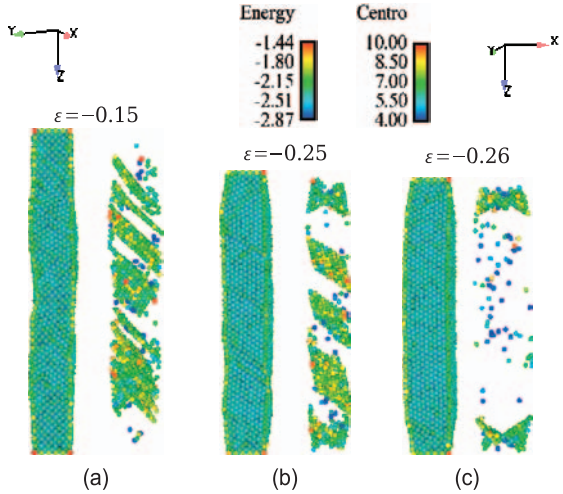

Fig. 2. The reorientation of an initially defect-free ⟨100⟩/{100} silver nanowire to a ⟨110⟩/{111} orientation free of interior defects at 500 K. Units of potential energy are in eV, centrosymmetry is defined in Ref. [50].

is shown in Figure 1. As illustrated in Figure 1(b), the reorientation occurs by spatially distributed twinning on different crystallographic variants. The interactions of the different twin boundaries results in the formation of parallel {111} stacking faults in the interior of the wire as shown in Figure 1(c). Upon completion of the reorientation in Figure 1(d), the parallel {111} stacking faults remain in the wire center, while additional twin-like defects exist at the ends of the wire. These defects exist due to the fact that the ends of the wire are constrained to move only in the z-direction during the reorientation in order to assure a clean tensile loading plane, and have been seen in previous simulations to propagate as twin boundaries to allow reversibility upon tensile loading to the initial, undeformed ⟨100⟩/{100} orientation.[31, 32]

The reorientation process leading to the ⟨110⟩/{111} silver nanowire containing only the twin boundaries at the wire ends is illustrated in Figure 2. Again, the compression induced by the tensile surface stresses causes reorientation via spatially distributed twinning, though on the same crystallographic variant as illustrated in Figures 2(a) and (b). Of note in both reorientation processes illustrated in Figures 1 and 2 is that the interior of the twins are largely defect-free; this confirms earlier investigations[31] indicating that the formation of defect-free twins is key to allowing reversibility between the ⟨110⟩/{111} and ⟨100⟩/{100} orientations. The final step in the reorientation is illustrated in Figures 2(b) and (c), which show that the remaining twin boundaries are removed by creation of ideal {111} surfaces, resulting in a ⟨110⟩/{111} wire without interior stacking faults.

A comparison between the defective and defect-free reoriented ⟨110⟩/{111} nanowires after further annealing to 30 K is shown in Figure 3. As can be seen, the defective ⟨110⟩/{111} nanowire has individual surface defects along with the interior {111} stacking faults. We note that

RESEARCH ARTICLE

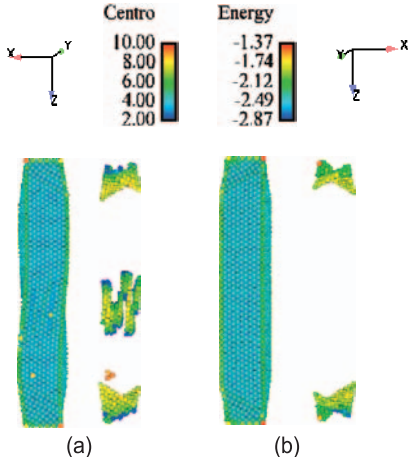

Fig. 3. Comparison of defective and defect-free ⟨110⟩/{111} nanowires after annealing to 30 K. Units of potential energy are in eV, centrosymmetry is defined in Ref. [50].

in the present examples, the defective and defect-free ⟨110⟩/{111} nanowires were obtained simply by small variations in the Nosé-Hoover frequency parameter, which causes the variations in twinning leading to the formation of interior {111} stacking faults seen in Figure 1. Variations in the Nosé-Hoover frequency lead to activation of slip planes at different points along the nanowire length due to disparities in local temperature, leading to the differences in the final structure of the reoriented ⟨110⟩/{111} nanowires seen in Figure 3.

While the differences in the ⟨110⟩/{111} nanowires were generated through small variations in numerical modeling, there are many practical situations in which variations in applied heat or energy could cause initial defects as shown in Figure 1. For example, if reorientation from ⟨100⟩/{100} to ⟨110⟩/{111} is initiated by application of heat, a non-uniform application of the heat source could activate different twinning planes and systems along the nanowire. In addition, if the shape memory nanowires are utilized as reinforcing materials within a nanocomposite, surface defects due to interactions with the matrix material could also adversely affect an idealized reorientation to a defect-free ⟨110⟩/{111} orientation. Because these shape memory nanowires are therefore likely to be utilized in situations where they are not defect-free, we will proceed in the next section to investigate the potentially deleterious effects existing defects have on their mechanical performance.

3.2. Uniaxial Tensile Deformation of Defective ⟨110⟩/{111} Silver Nanowires

3.2.1. Uniaxial Deformation at 30 K

In this section, the results of the MD simulations of the uniaxial tensile loading for the defective ⟨110⟩/{111} silver nanowires at 30 K are discussed. The loading was performed across three decades of applied strain rates at 30 K considering both idealized adiabatic and isothermal heat transfer conditions. Strain is defined as $\epsilon = \frac{l-l_0}{l}$, where l_0 is the length of the reoriented ⟨110⟩/{111} silver nanowires with initial {111} stacking faults and l is the current length of the nanowire during loading. Stresses reported in this work are based on the virial theorem, which takes the form

$$\sigma_{ij} = \frac{1}{V}\left(\frac{1}{2}\sum_{\alpha=1}^{N}\sum_{\beta\neq\alpha}^{N} U'(r^{\alpha\beta})\frac{\Delta x_i^{\alpha\beta}\Delta x_j^{\alpha\beta}}{r^{\alpha\beta}} - \sum_{\alpha=1}^{N} m_\alpha \dot{x}_i^\alpha \dot{x}_j^\alpha\right) \quad (2)$$

where V is the current volume of the nanowires, N is the total number of atoms, $\dot{x}_i^\alpha$ is the ith component of velocity for atom α, m_α is the mass of atom α, $r^{\alpha\beta}$ is the distance between two atoms α and β, $\Delta x_j^{\alpha\beta} = x_j^\alpha - x_j^\beta$, U is the potential energy function and $r^{\alpha\beta} = \|\Delta x_j^{\alpha\beta}\|$. Alternative methods of defining stress in an atomistic system have been recently proposed in.[51, 52]

We present in Figure 4 an illustration of the stress-induced reorientation from ⟨110⟩/{111} to ⟨100⟩/{100} that is possible even if the ⟨110⟩/{111} nanowire is initially defective. The applied strain rate is $\dot{\epsilon} = 10^8$ and the wire is loaded adiabatically at 30 K. Upon application of tensile loading, the {111} stacking faults in the wire center first reorient into two separate twin boundaries as illustrated in Figure 4(b). Concurrently, the twin-like defects at the wire ends from the opposite ends of the twin boundaries; the two twins then propagate towards each other under tensile loading as shown in Figure 4(c). At this point in the deformation, the interior of the twins have a ⟨110⟩ orientation with {111} side surfaces. Outside the twin boundaries, the wire has its initial ⟨100⟩/{100} orientation with {100} side surfaces.[30, 31] At a strain of $\epsilon = 0.38$

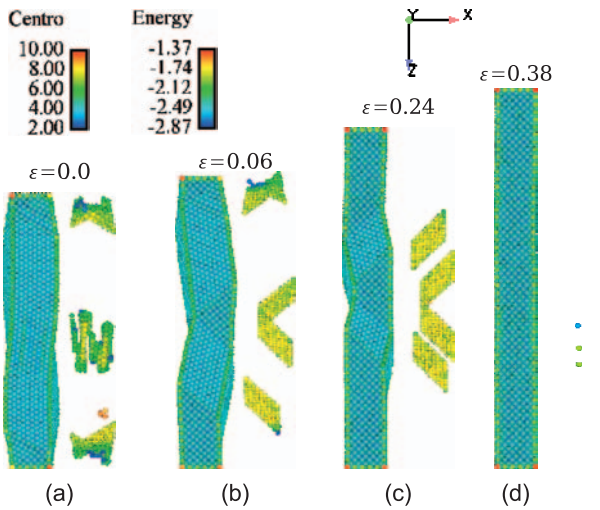

Fig. 4. Stress-induced reorientation from ⟨110⟩/{111} at zero strain to ⟨100⟩/{100} orientation at about 38 percent strain for adiabatically loaded silver nanowire at $\dot{\epsilon} = 10^8$. Units of potential energy are in eV, centrosymmetry is defined in Ref. [50].

RESEARCH ARTICLE

with respect to initial ⟨110⟩/{111} nanowire, the two sets of twins annihilate each other and the nanowire regains its initial, defect-free ⟨100⟩/{100} orientation as seen in Figure 4(d).

A unique feature in the deformation of the initially defective nanowire seen in Figure 4 is the formation and propagation of two distinct twins within the nanowire interior, which is in contrast to the single twin boundary propagation seen in defect-free nanowires.[30–32] Previous investigations into the uniaxial deformation of defect-free silver shape memory nanowires found that the propagation of multiple twins was seen only in extremely high strain-rate loading conditions,[32] indicating that such deformation proceeds as a way of relieving the local material instability. In addition, the propagation of multiple twins in defect-free wires was seen to result in higher plateau stresses driven by the increased effort necessary to propagate the multiple twin boundaries.

In this work, we define the transformation stress as the difference between the initial stress in the wire prior to tensile loading and the maximum stress during the initial period of linear elastic deformation, while the plateau stress is defined as the stress state present in the wire immediately following the transformation stress as the reorientation from ⟨110⟩/{111} to ⟨100⟩/{100} proceeds via the propagation of the twin boundaries. Due to the non-constant plateau stresses seen in this work, we loosely define the plateau period as ending at about $\epsilon = 0.30$. In terms of the active deformation mechanisms illustrated in this work, the transformation stress corresponds to the stress level at which the initial {111} stacking faults in the defective nanowires orient themselves favorably under the applied uniaxial loading to form the appropriate twin boundaries.

The stress–strain curves for the defective nanowire at 30 K under both adiabatic and isothermal loading conditions across three decades of strain rates are shown in Figure 5. The curves illustrate many interesting features particular to the tensile deformation of the ⟨110⟩/{111} nanowires with initial {111} stacking faults, which we will now discuss.

The first phenomena we discuss deals with the fact that, for both adiabatic and isothermal deformation, we do not observe a flat stress plateau following the transformation stress as typically exists in polycrystalline SMAs,[39, 53] and was observed in the uniaxial tensile deformation of defect-free ⟨110⟩/{111} shape memory nanowires.[32] In polycrystalline SMAs, the flat stress plateau following the transformation stress occurs while favorably oriented austenite grains transform under applied loading to martensite. In defect-free shape memory nanowires, the flat stress plateau occurs after a sufficiently high stress state (the transformation stress) is reached whereby the twin boundaries at the ends of the wire as illustrated in Figure 2 begin to propagate.

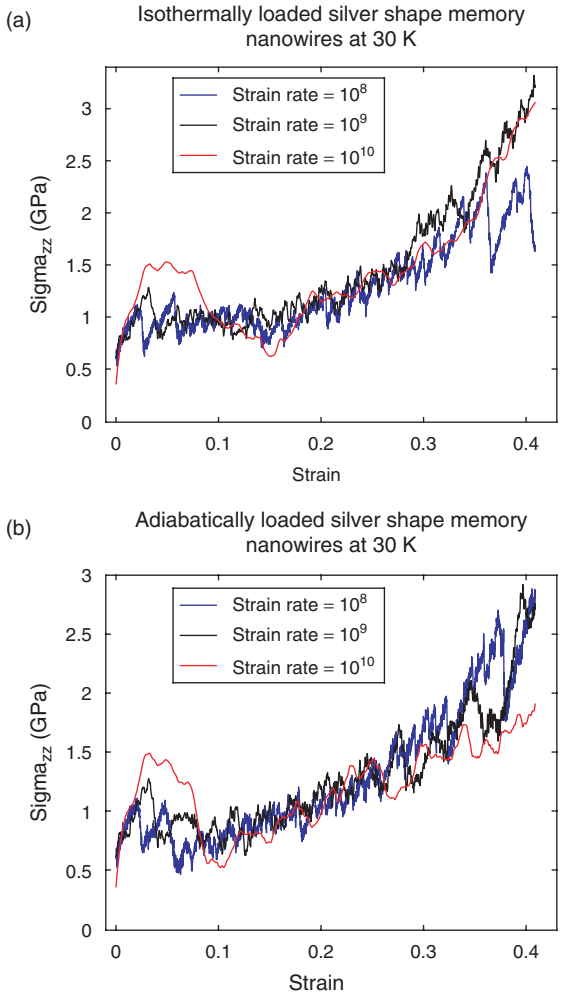

Fig. 5. The uniaxial stress–strain relationship under various loading rates for silver shape memory nanowires at 30 K. (a) Isothermal, (b) adiabatic.

In the ⟨110⟩/{111} nanowires with initial {111} stacking faults, multiple twins initiate and propagate as seen in Figures 4(b–c). Due to the presence of the twin boundaries, long-ranged stress fields exist in the nanowire. The propagation of the multiple twin boundaries causes interaction of the stress fields, and results in a non-constant and increasing stress level necessary to propagate the multiple twin boundaries. This is observed in Figure 5, which illustrates that from a strain level of about $\epsilon = 0.1$, the plateau stress is non-constant and increasing for the adiabatically loaded wires, while a similar transition occurs at a strain level of about $\epsilon = 0.15$ in the isothermally loaded wires. The later increase in plateau stress in the isothermal case is due to difficulties in untangling the {111} stacking fault structure in the wire interior. The slope of the stress–strain curve increases markedly at higher strains due to the stress needed to annihilate and drive together the twin boundaries; this is most evident for the isothermally loaded nanowires beginning at a strain level of about $\epsilon = 0.30$ in Figure 5(a).

RESEARCH ARTICLE

This conclusion has been drawn by comparing the present results to stress–strain curves of the tensile deformation of defect-free ⟨110⟩/{111} shape memory nanowires, in which the plateau stress remains constant across a range of deformation temperatures and heat transfer conditions to strain levels of 25 to 30 percent while the single twin boundaries propagate towards each other.[32] The stress in the defect-free wires begins to increase once the stress fields due to the boundaries of the single propagating twin begin to interact. The interaction culminates with the annihilation of the twin boundaries, and the twin boundary interaction/annihilation process results in a nearly monotonically increasing stress strain-response. Because of the single twin system propagating in the defect-free wires, the plateau stress remains constant for a larger duration of time, thus explaining the difference in observed stress–strain response between defective and defect-free ⟨110⟩/{111} shape memory nanowires loaded under tension.

A second point of interest is related to one of the major purposes for initiating this work, which is to determine whether the existence of initial defects within the ⟨110⟩/{111} nanowires prevents complete reorientation back to the original ⟨100⟩/{100} orientation. As can be seen in Figure 5 for the 30 K cases, most wires considered were able to reorient back to the defect-free ⟨100⟩/{100} orientation. Two exceptions were seen: the wire loaded isothermally at a strain rate of $\dot{\epsilon} = 10^8$ and the wire loaded adiabatically at a strain rate of $\dot{\epsilon} = 10^{10}$. As we will show later in this work, the wires loaded at lower temperatures and strain rates are more likely to reorient back to the ⟨100⟩/{100} configuration at lower temperatures.

For those ⟨110⟩/{111} nanowires with initial defects that were able to reorient back to the defect-free ⟨100⟩/{100} orientation, the mechanical properties are nearly identical to those seen in the defect-free ⟨110⟩/{111} case. For example, the stress in the wires when the ⟨100⟩/{100} orientation is reached exceeds 3 GPa in the isothermal cases at 30 K, and is slightly below 3 GPa in the adiabatic cases, similar to what was previously observed for defect-free wires.[32] The transformation stresses and strains are reduced for the initially defective wires; this will be discussed in detail in the next section.

The thermal softening observed in the tangent moduli in Figure 5 after the plateau stress raises an interesting and enlightening comparison of nanowire shape memory behavior and bulk, polycrystalline shape memory behavior. In polycrystalline SMAs, the shape memory effect occurs due to a phase transformation between the low temperature martensite phase and the high temperature austenite phase. Because the austenite phase is stable at high temperatures, raising the deformation temperature requires more stress to induce and propagate the martensitic phase transformation due to the fact that the material is closer to stability in the austenite phase.

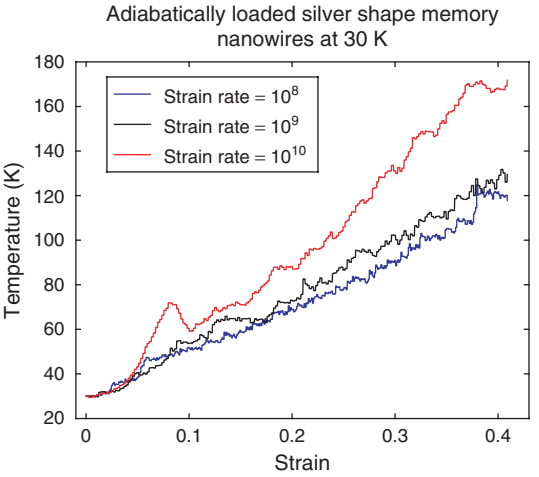

Fig. 6. Evolution of temperature for three decades of applied strain rates in adiabatically loaded silver shape memory nanowires at an initial temperature of 30 K.

For the adiabatic loading shown here, the temperature increases dramatically during the deformation as illustrated in Figure 6. In addition, it has been documented that a critical temperature T_c is required to reorient the ⟨100⟩/{100} nanowire to the ⟨110⟩/{111} wires that are uniaxially loaded in this work. Thus, it would appear that shape memory nanowires should behave similarly to polycrystalline SMAs in that at the higher nanowire temperatures that result due to the adiabatic loading conditions, the stresses in the nanowires should increase to offset the increased tendency of the nanowire to revert back to the lower energy ⟨110⟩/{111} orientation. However, as shown in Figure 5, the stress when the initial ⟨100⟩/{100} orientation is reached is still lower than when the nanowire is loaded isothermally. It thus appears that at the nanoscale, thermal fluctuations which draw the lattice structure away from an idealized crystalline state have a much stronger effect on the resulting nanowire mechanical strength and properties than energetic considerations drawing the nanowire to various crystallographic orientations.

3.2.2. *Uniaxial Deformation at Elevated Temperatures*

In this section, the response of defective ⟨110⟩/{111} nanowires under uniaxial tension at elevated temperatures is discussed in comparison to the 30 K cases. Similar to the nanowires at 30 K, these nanowires were tested under various loading rates and heat transfer conditions for a given deformation temperature. The similarities and differences between the thermomechanical behavior of the ⟨110⟩/{111} nanowires with initial defects at elevated temperatures as compared to lower temperatures are best illustrated by considering the stress–strain responses, which are shown in Figures 7 and 8.

The major similarities as compared to the mechanical behavior at lower temperatures are the increasing and nonconstant plateau stress as a function of strain, and the

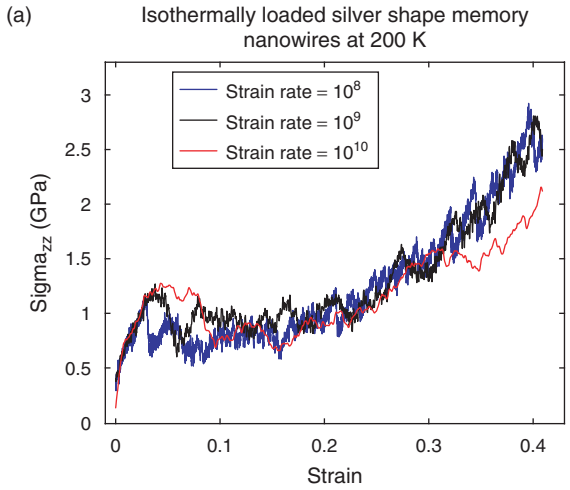

Fig. 7. The uniaxial stress–strain relationship under various loading rates for silver shape memory nanowires at 200 K. (a) Isothermal, (b) adiabatic.

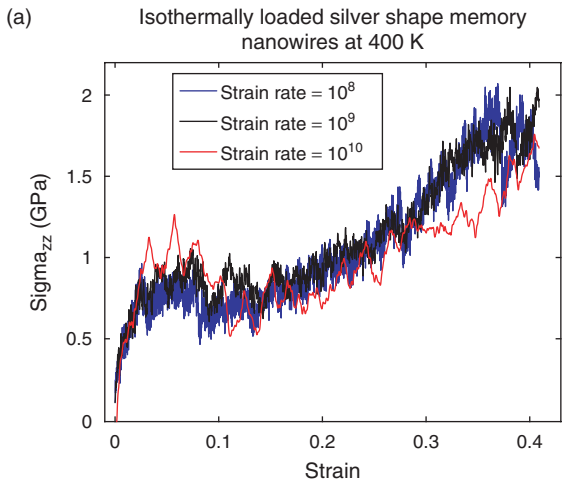

Fig. 8. The uniaxial stress–strain relationship under various loading rates for silver shape memory nanowires at 400 K. (a) Isothermal, (b) adiabatic.

thermally-induced softening of the reorientation stress, or the stress level in the nanowires after the reorientation to the ⟨100⟩/{100} configuration has been completed. The increasing plateau stress occurs for the same reason as previously discussed, i.e., due to the propagation and interaction of multiple twins within the nanowire. The reduced reorientation stress occurs similarly due to thermal softening effects on the overall mechanical strength.

One important difference at 400 K is that none of the initially defective ⟨110⟩/{111} nanowires, regardless of applied strain rate or heat transfer condition, are able to complete a defect-free stress-induced reorientation back to the initial ⟨100⟩/{100} configuration. The cause for this is illustrated in Figure 9. At 400 K, the reorientation generally proceeds with multiple twin boundaries propagating under applied uniaxial loading, and reaches a state just before twin boundary annihilation should occur, as illustrated in Figure 9(a). At this point, partial dislocations propagate through the wire leaving trailing stacking faults, as observed in Figure 9(b). One of the twins may eventually annihilate, as does the upper twin in Figure 9(c), but the other remains and additional partial dislocations propagate through the wire, preventing defect-free reorientation back to the initial ⟨100⟩/{100} configuration. Because this occurs more frequently at elevated temperatures and strain rates, it is likely that reduced energetic barriers to defect nucleation in conjunction with surface defects are the cause for premature yielding before defect-free reorientation can occur.

3.3. Discussion: Overall Impact of Initial Defects

One manner in which the effects of initial defects can be quantified is by looking at the transformation stresses and strains in the tensile-loaded ⟨110⟩/{111} nanowires. For example, we observe differences in the transformation stresses and strains at elevated temperatures versus those at lower temperatures, and also in comparison to the transformation stresses and strains observed in the defect-free wires; these are quantified graphically in Figures 10 and 11 for isothermally loaded defect-free and defective ⟨110⟩/{111} nanowires. All references to and data

RESEARCH ARTICLE

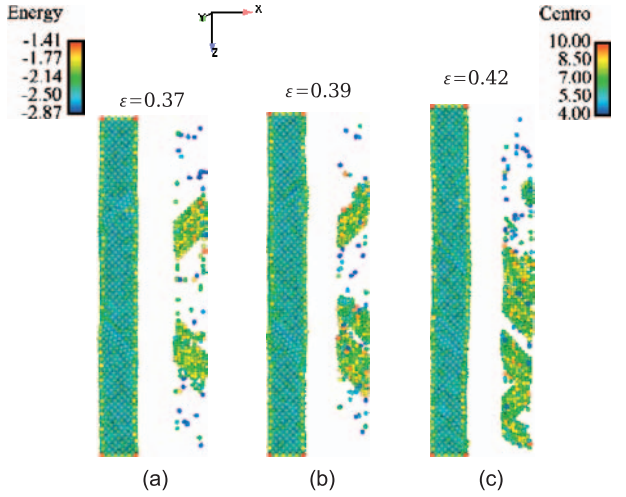

Fig. 9. Adiabatic tensile loading of an initially defective ⟨110⟩/{111} nanowire at 400 K and a strain rate of $\dot{\epsilon} = 10^9$ in which defect-free reorientation to ⟨100⟩/{100} does not occur. Units of potential energy are in eV, centrosymmetry is defined in Ref. [50].

for defect-free ⟨110⟩/{111} wires are taken from Park and Ji.[32]

Similar trends are seen in the adiabatically loaded wires. The first observable trend is that the transformation stresses and strains both tend to increase with increasing temperature for the initially defective ⟨110⟩/{111} nanowires. The reason for this is tied to the initial stress state in the wires due to the presence of the initial defects. As illustrated in Figures 5, 7, and 8 the stress in the initially defective ⟨110⟩/{111} wires is nonzero after thermal annealing. With increasing temperature, the initial stress in the wires gradually approaches zero. Therefore, while the transformation stress itself decreases with increasing temperature, the difference between the initial stress state and the transformation stress increases with temperature.

This fact also explains the increase in transformation strain with increasing temperature. That is, the increase in initial temperature allows the wire to accommodate the initial {111} stacking faults by thermally-induced expansion. Upon application of tensile loading, the wire is then allowed to deform elastically for a longer period of time before the stress state in the wire reaches the critical transformation value, causing the initial stacking faults to reorient into propagating twin boundaries. In this sense, the behavior of the ⟨110⟩/{111} nanowires with initial defects is similar to that observed in polycrystalline SMAs, in which the transformation stresses and strains are observed to increase with increasing temperature. The initial stacking faults then serve as idealized grain boundaries, which require additional work to transform into propagating twins to initiate the stress-induced reorientation.

In contrast, as illustrated in Figure 10(a), the transformation stress for the defect-free ⟨110⟩/{111} nanowires

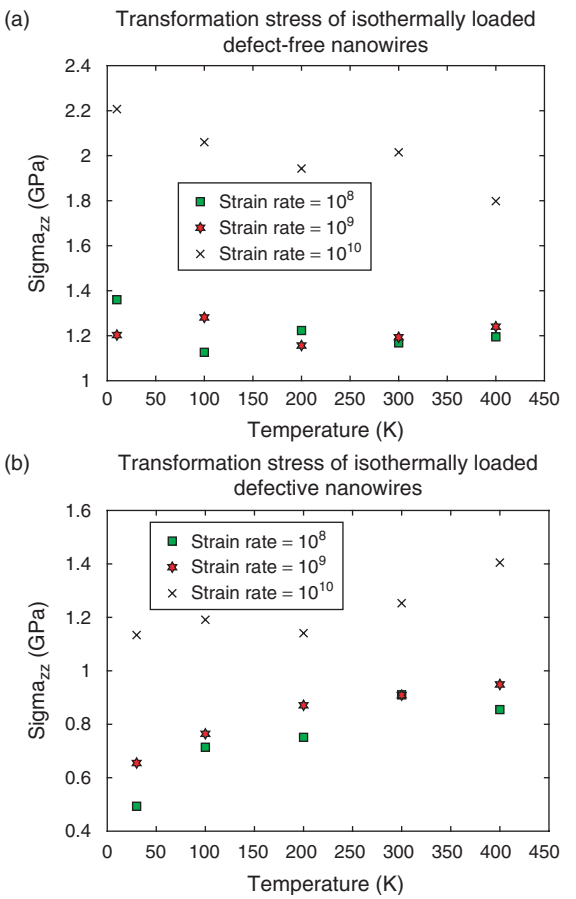

Fig. 10. Summary of transformation stresses as a function of temperature for: (a) Defect-free ⟨110⟩/{111} nanowires. (b) ⟨110⟩/{111} nanowires with initial {111} stacking faults.

appears to decrease or remain constant with temperature for most cases, again indicating thermal softening effects on reducing the amount of idealized deformation that is supportable in the nanowires. The transformation strains for the defect-free wires also show patterns of inconsistency, particularly at temperatures approaching the critical temperature for the ⟨100⟩/{100} to ⟨110⟩/{111} reorientation; see Figure 11(a). Despite these trends, we note that for a given temperature and strain rate, the transformation stresses and strains for the defect-free wires were in all cases larger than those for the initially defective wires, indicating the effects of the initial defects in reducing these values.

The simulation results have also revealed both similarities and differences in the tensile stress–strain responses of the initially defective ⟨110⟩/{111} nanowire studied in this work and the defect-free ⟨110⟩/{111} nanowires.[32] For example, the transformation stresses and strains shown in Figures 10 and 11 were lower for all temperatures and loading rates for the initially defective wires. However, once the stress state in the wire had increased enough to initiate the propagation of multiple twins, the plateau stresses and the stress state in the wires when the

RESEARCH ARTICLE

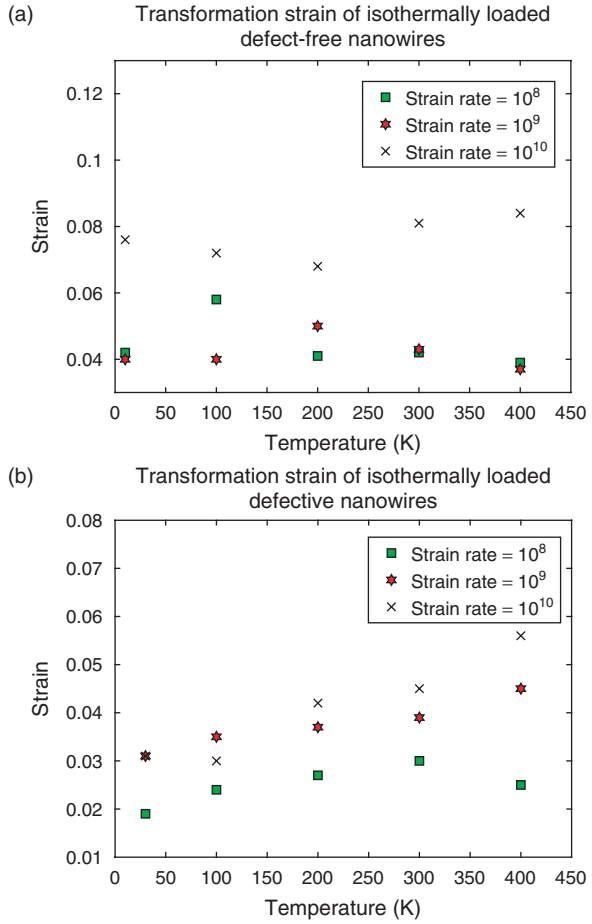

Fig. 11. Summary of transformation strains as a function of temperature for: (a) Defect-free ⟨110⟩/{111} nanowires. (b) ⟨110⟩/{111} nanowires with initial {111} stacking faults.

original ⟨100⟩/{100} orientation was reached is similar between initially defective and defect-free ⟨110⟩/{111} nanowires.[32] In addition, when irreversible deformation was observed to occur in the wires due to the formation of complex stacking fault structures at twin boundaries or full dislocations, the irreversibility occurred late in the reorientation process, typically after strains of 30 percent or larger with respect to the original ⟨110⟩/{111} configuration; this is illustrated in Figure 9. This result is quite encouraging, as most polycrystalline SMAs have reversible inelastic strains approaching about 10 percent.[38]

Another interesting aspect of the deformation is that the stress state during the uniaxial tensile deformation when multiple twins propagate in the nanowires, as was observed throughout this work for the initially defective wires, is not higher than the stress observed in the uniaxial tensile deformation of the defect-free wires. The reason for this can be tied to the reduced velocities at which multiple twins propagate in a wire of the same length as compared to the velocity of a single propagating twin. As was eloquently explained by Shaw and Kyriakides,[39] if more twins are propagating in a material of a given length, the velocities of each set of twins must be reduced accordingly to accommodate the same amount of deformation. Therefore, while a larger stress is presumably required to propagate multiple twins as compared to a single twin, the fact that the velocities of the propagating twins are reduced accounts for the non-elevated stress response for initially defective shape memory nanowires as compared to initially defect-free wires.

We close this discussion by mentioning two key issues which were not considered in this work. First, an issue not considered in this work, but which can be inferred from the results herein is the importance of stochastic effects in predicting the resulting mechanical properties of defective shape memory nanowires. The configuration chosen in this work, i.e., that of the reoriented ⟨110⟩/{111} nanowire with internal {111} stacking faults, was analyzed after considerable work studying the ⟨100⟩/{100} to ⟨110⟩/{111} reorientation, and finding the most typical configuration with defects to be that with interior {111} stacking faults. Clearly, this single situation does not account for all possible scenarios involving combinations of initial defects both within the nanowire and on the nanowire surfaces. However, it does serve to illustrate that with judicious selections of deformation temperature and applied strain rate, nanowires with initial defects can still reorient completely between the low energy ⟨110⟩/{111} and higher energy ⟨100⟩/{100} orientations, thus paving the way for shape memory behavior and relevant applications at the nanoscale.

Finally, another key issue which was not considered in the present work but has important implications for practical usage of metal nanowires is that of oxidation. In the future, it will be important to investigate, perhaps using first principles techniques for accuracy, the effects of oxidation layers on the deformation behavior and properties of metallic nanowires and nanostructures.

4. SUMMARY AND CONCLUSIONS

We have presented atomistic simulations of the stress-induced reorientation for silver shape memory nanowires between a ⟨110⟩/{111} orientation with interior {111} stacking faults and a ⟨100⟩/{100} orientation. The simulations were performed accounting for various deformation temperatures, idealized heat transfer conditions and loading rates to investigate the deleterious effects of initial defects on the robustness of the shape memory effect in silver nanowires. Though the reorientation was shown to be precluded in certain situations, notably at deformation temperatures approaching the critical reorientation temperature T_c and high applied strain rates, the nanowires in general demonstrated reversibility at lower strain rates and deformation temperatures.

Due to the existence of the initial {111} stacking faults, reversibility between the ⟨110⟩/{111} and ⟨100⟩/{100} orientations was shown to occur by the propagation and annihilation of multiple twin boundaries. While

RESEARCH ARTICLE

the transformation stresses and strains of the initially defective ⟨110⟩/{111} wires were reduced as compared to initially defect free ⟨110⟩/{111} wires, the formation and evolution of multiple twin boundaries during tensile loading led to non-constant and increasing plateau stresses as compared to previous investigations of initially defect-free ⟨110⟩/{111} nanowires with a single propagating twin boundary.[32] It was also shown that if reorientation to the ⟨100⟩/{100} configuration occurred, the nanowires with initial defects showed no degradation in mechanical properties as compared to those without initial defects.

While the simulations in this work focused on the behavior of silver nanowires, it would be of great interest to study the reorientation tendencies and non-idealized deformation characteristics of other FCC metals that have been shown to exhibit shape memory and pseudoelastic behavior, namely copper[29–31] and nickel.[31] This would be of interest as those materials have significantly higher stacking fault energies than silver, which may impact the twinning mechanisms observed in this work. In addition, while the silver shape memory nanowires tended to deform reversibly up to at least 30 percent strain, the viability of that strain figure under repeated cyclic loading needs to be carefully evaluated.

Acknowledgments: The authors gratefully acknowledge funding from the Vanderbilt University Discovery Grant in support of this research.

RESEARCH ARTICLE

References

1. C. M. Lieber, *MRS Bulletin* 28, 486 (**2003**).
2. N. I. Kovtyukhova and T. E. Mallouk, *Chemistry-A European J.* 8, 4355 (**2002**).
3. P. Yang, *MRS Bulletin* 30, 85 (**2005**).
4. Y. Xia, P. Yang, Y. Sun, Y. Wu, B. Mayers, B. Gates, Y. Yin, F. Kim, and H. Yan, *Adv. Mater.* 15, 353 (**2003**).
5. B. Wu, A. Heidelberg, and J. J. Boland, *Nature Mater.* 4, 525 (**2005**).
6. S. Cuenot, C. Frétigny, S. Demoustier-Champagne, and B. Nysten, *Phys. Rev. B* 69, 165410 (**2004**).
7. G. Y. Jing, H. L. Duan, X. M. Sun, Z. S. Zhang, J. Xu, Y. D. Li, J. X. Wang, and D. P. Yu, *Phys. Rev. B* 73, 235409 (**2006**).
8. H. Ikeda, Y. Qi, T. Cagin, K. Samwer, W. L. Johnson, and W. A. G. III, *Phys. Rev. Lett.* 82, 2900 (**1999**).
9. U. Landman, W. D. Luedtke, N. A. Burnham, and R. J. Colton, *Science* 248, 454 (**1990**).
10. P. S. Branicio and J. P. Rino, *Phys. Rev. B* 62, 16950 (**2000**).
11. P. Walsh, W. Li, R. K. Kalia, A. Nakano, P. Vashista, and S. Saini, *Appl. Phys. Lett.* 78, 3328 (**2001**).
12. J.-W. Kang and H.-J. Hwang, *Nanotechnology* 12, 295 (**2001**).
13. H. A. Wu, A. K. Soh, X. X. Wang, and Z. H. Sun, *Key Engrg. Mater.* 261–263, 33 (**2004**).
14. W. Liang and M. Zhou, Response of copper nanowires in dynamic tensile deformation. *Proceedings of the Institution of Mechanical Engineers, Part C: J. Mech. Engrg. Sci.* 218, 599 (**2004**).
15. D. Sanchez-Portal, E. Artacho, J. Junquera, P. Ordejon, A. Garcia, and J. M. Soler, *Phys. Rev. Lett.* 83, 3884 (**1999**).
16. E. Z. da Silva, A. J. R. da Silva, and A. Fazzio, *Phys. Rev. Lett.* 87, 256102 (**2001**).
17. H. S. Park and J. A. Zimmerman, *Phys. Rev. B* 72, 054106 (**2005**).
18. C. Ji and H. S. Park, *Appl. Phys. Lett.* 89, 181916 (**2006**).
19. A. S. J. Koh and H. P. Lee, *Nano Lett.* 6, 2260 (**2006**).
20. H. Mehrez and S. Ciraci, *Phys. Rev. B* 56, 12632 (**1997**).
21. K. Gall, J. Diao, and M. L. Dunn, *Nano Lett.* 4, 2431 (**2004**).
22. J. Diao, K. Gall, and M. L. Dunn, *Nano Lett.* 4, 1863 (**2004**).
23. P. Z. Coura, S. G. Legoas, A. S. Moreira, F. Sato, V. Rodrigues, S. O. Dantas, D. Ugarte, and D. S. Galvao, *Nano Lett.* 4, 1187 (**2004**).
24. H. S. Park and J. A. Zimmerman, *Scripta Materialia* 54, 1127 (**2006**).
25. H. S. Park, K. Gall, and J. A. Zimmerman, *J. Mech. Phys. Solids* 54, 1862 (**2006**).
26. J. Diao, K. Gall, and M. L. Dunn, *Nature Mater.* 2, 656 (**2003**).
27. K. Gall, J. Diao, M. L. Dunn, M. Haftel, N. Bernstein, and M. J. Mehl, *J. Engrg. Mater. Technol.* 127, 417 (**2005**).
28. J. Diao, K. Gall, and M. L. Dunn, *Phys. Rev. B* 70, 075413 (**2004**).
29. W. Liang and M. Zhou, *J. Engrg. Mater. Technol.* 127, 423 (**2005**).
30. W. Liang, M. Zhou, and F. Ke, *Nano Lett.* 5, 2039 (**2005**).
31. H. S. Park, K. Gall, and J. A. Zimmerman, *Phys. Rev. Lett.* 95, 255504 (**2005**).
32. H. S. Park and C. Ji, *Acta Materialia* 54, 2645 (**2006**).
33. Y. Wang, S. Teitel, and C. Dellago, *Nano Lett.* 5, 2174 (**2005**).
34. R. C. Cammarata, *Progress in Surface Science* 46, 1 (**1994**).
35. Y. Kondo and K. Takayanagi, *Phys. Rev. Lett.* 79, 3455 (**1997**).
36. M. I. Haftel and K. Gall, *Phys. Rev. B* 74, 035420 (**2006**).
37. H. S. Park, *Nano Lett.* 6, 958 (**2006**).
38. K. Otsuka and X. Ren, *Progress in Materials Science* 50, 511 (**2005**).
39. J. A. Shaw and S. Kyriakides, *J. Mech. Phys. Solids* 43, 1243 (**1995**).
40. L. C. Brinson, I. Schmidt, and R. Lammering, *J. Mech. Phys. Solids* 52, 1549 (**2004**).
41. A. Leach, Molecular Modelling: Principles and Applications, Pearson Education Limited (**2001**).
42. M. S. Daw and M. I. Baskes, *Phys. Rev. B* 29, 6443 (**1984**).
43. M. S. Daw, S. M. Foiles, and M. I. Baskes, *Materials Science Reports* 9, 251 (**1993**).
44. A. F. Voter, Embedded atom method potentials for seven fcc metals: Ni, Pd, Pt, Cu, Ag, Au, and Al. Los Alamos Unclassified Technical Report LA-UR 93-3901.
45. S. Nosé, *J. Chem. Phys.* 81, 511 (**1984**).
46. W. G. Hoover, *Phys. Rev. A* 31, 1695 (**1985**).
47. S. J. Plimpton, *J. Computat. Phys.* 117, 1 (**1995**).
48. Warp, http://www.cs.sandia.gov/~sjplimp/lammps.html
49. P. H. Leo, T. W. Shield, and O. P. Bruno, *Acta Metallurgica et Materialia* 41, 2477 (**1993**).
50. C. L. Kelchner, S. J. Plimpton, and J. C. Hamilton, *Phys. Rev. B* 58, 11085 (**1998**).
51. M. Zhou, A new look at the atomic level virial stress: on continuum-molecular equivalence. *Proceedings of the Royal Society of London Series A-Mathematical, Physical and Engineering Sciences* 459, 2347 (**2003**).
52. J. A. Zimmerman, E. B. W. III, J. J. Hoyt, R. E. Jones, P. A. Klein, and D. J. Bammann, *Modelling and Simulation in Materials Science and Engineering* 12, S319 (**2004**).
53. P. Sittner, Y. Liu, and V. Novak, *J. Mech. Phys. Solids* 53, 1719 (**2005**).

Received: 21 August 2006. Accepted: 7 November 2006.